RSC Advances

PAPER

Cite this: *RSC Adv.*, 2015, **5**, 24528

Catalyst-free synthesis of carbon nanospheres for potential biomedical applications: waste to wealth approach†

Shoriya Aruni Abdul Manaf,[a] Partha Roy,[b] Korada V. Sharma,[c] Zainab Ngaini,[d] Victor Malgras,[e] Ali Aldalbahi,[f] Saad M. Alshehri,[f] Yusuke Yamauchi[e] and Gurumurthy Hegde*[ag]

Received 17th November 2014
Accepted 24th February 2015

DOI: 10.1039/c4ra14693j

www.rsc.org/advances

A single step and simple pyrolysis technique is used to prepare carbon nanospheres (CNSs) from natural biowaste sago hampas in a nitrogen atmosphere without any catalyst. Scanning electron microscope (SEM) images along with transmission electron microscope (TEM) images show evidence of high quality CNSs with a good particle size uniformity. Both X-ray diffraction (XRD) and Raman data show the presence of graphitic characteristic peaks of CNSs. Zeta-potential study reveals that the obtained CNSs can be well dispersed in solution making them suitable for cell imaging applications. The use of biowaste sago hampas is very important from the viewpoint of sustainable synthesis of functional CNSs for the future.

Introduction

Carbon nanomaterials with different shapes and structures have attracted widespread attention from many researchers working in various fields around the globe due to their vast applications in diverse fields such as catalyst supports,[1] anode materials of Li-ion batteries,[2] nanostructures in diagnosis,[3] and multiphoton bioimaging.[4] For imaging and efficient drug delivery, various carbon-based nanomaterials have been used as drug delivery vehicles, often tagged with some fluorescent agents and antibodies.[5–7] Different forms of carbon nanostructures, including carbon nanotubes,[8,9] carbon nanofibers,[10,11] carbon trees,[12,13] carbon spheres,[14,15] mesoporous carbons,[16] carbon capsules,[17] and carbon nanowalls[18] have been developed since the last 20 years. Among various shapes, carbon nanospheres (CNSs) are gaining interest as catalyst supports, fillers for polymer nanocomposites, column packing and lubricating materials, biomedical drug carriers, *etc.* In recent reports, the CNSs also exhibited excellent photoluminescent properties.[19–21]

Various synthetic approaches have been reported to prepare CNSs.[22–25] All of the methods for carbonization involve the use of either a template, a catalyst, or an oxidising agent. The templating methods require time-consuming process to collect only pure CNSs by separating the material from the used catalysts. Graphite powders, petroleum pitch, carbon rich polymers, and other kinds of liquid/gaseous hydrocarbons have been extensively used for the synthesis of CNSs as precursor. As these chemicals becoming scarce resources and have detrimental impacts on the environment, the use of alternative carbon sources for the synthesis of carbonaceous materials is in high demand in various fields. Thus, the carbon source and the synthetic method are the two key issues for the development of environment-friendly and cost-effective preparation of CNSs. Plant biomasses, biobased oils, and hydrocarbons may serve as the best alternative and renewable carbon sources. Very less effort has been made in this regard to prepare CNSs,[26,27] although the biomasses have been utilized for the synthesis of chemicals through green routes.[28]

This encouraged us to search for new carbon sources and very recently we reported CNSs from oil palm leaves and its electrochemical applications.[29] Following the urge to find new carbon sources for the preparation of CNSs, herein we propose the use of bio-waste sago 'hampas' which is an inexpensive fibrous residue obtained from sago palm tree. Sago hampas are rich in cellulose and hemicelluloses with small percentage of lignin content and have a porous structure.[27b,30] The porous nature of sago hampas prompted us to prepare new CNSs by a

[a]*Faculty of Industrial Sciences and Technology, Universiti Malaysia Pahang, 26300 Gambang, Kuantan, Malaysia. E-mail: murthyhegde@gmail.com*

[b]*Faculty of Engineering Technology, Universiti Malaysia Pahang, 26300 Gambang, Kuantan, Malaysia*

[c]*Department of Mechanical Engineering, Faculty of Engineering, University Technology PETRONAS, Bandar Seri Iskandar, 31750, Tronoh, Perak, Malaysia*

[d]*Department of Chemistry, Faculty of Resource Science and Technology, Universiti Malaysia Sarawak, 94300 Sarawak, Malaysia*

[e]*World Premier International (WPI) Research Center for Materials Nanoarchitectonics (MANA), National Institute for Materials Science (NIMS), 1-1 Namiki, Tsukuba, Ibaraki 305-0044, Japan*

[f]*Department of Chemistry, College of Science, King Saud University, Riyadh 11451, Saudi Arabia*

[g]*BMS R and D Centre, BMSCE, Bull Temple Road, 560019 Bangalore, India*

† Electronic supplementary information (ESI) available: See DOI: 10.1039/c4ra14693j

simple and catalyst-free pyrolysis technique. The present method is indeed inexpensive and environmentally friendly. Also, our approach can be used in the development of promising applications in various fields.

Experimental section

Synthesis and purification of CNSs

The dry sago hampas were collected from local sago palm estate in Malaysia. The fibrous residue was separated and dried in an oven at 110 °C for two days to remove all the moisture. The dry sago hampas were crushed and grinded at a speed of 12 000 rpm using a centrifugal mill (Retsch, ZM 200, Germany). The grinded raw sago hampas was then sieved to a particle size of 62 μm. Afterwards, the filtered material was pyrolyzed in a tube furnace (Nabertherm, EW-33334-36) at 400 °C or 600 °C for 2 hours under the continuous flow of N_2 (150 mL cm^{-3}) at a heating rate of 5 °C min^{-1} and subsequently cooled down to room temperature in the N_2 atmosphere. The obtained pyrolyzed product was finally washed with a 1 M HCl solution and then rinsed with deionized water.

Characterization

The raw sago hampas and CNSs were characterized using Perkin Elmer Spectrum 100/FT-IR, SEM with EDX analysis (JEOL/JSM-7800F), XRD (Rigaku/Mineflex II), TEM (JEOL/JSM 1230), and TGA (METTLER TOLEDO/TGA/DSC HT/1600). The BET surface area was evaluated using Micromeritics ASAP 2020. Before the measurement, the CNSs were degased for 12 hours at 200 °C. The Raman spectra of CNSs were taken using HORIBA Scientific Raman spectroscopy. The zeta potentials were measured by Malvern Mastersizer 2000 (Zetasizer Nano ZS90, Malvern Instruments Ltd., UK). Zeta potential is an indicator of the surface charge and colloidal stability of particles. Freshly prepared CNSs were appropriately diluted in aqueous solution just before the measurement. All measurements were carried out at room temperature after 10 min of equilibration. The data were averaged over three measurements.

Results and discussion

TG–DTA curves of the precursor sago hampas reveal that the degradation takes place in a single step. The mass degradation starts at 270 °C and complete degradation takes place around 360 °C (Fig. S1†). Based on this, we follow a green method for the synthesis of CNSs by a convenient and harmless catalyst-free pyrolysis technique. SEM observation combined with energy dispersive X-ray (EDX) of the precursor sago hampas was carried out to know the original shape and the mass ratios of carbon along with other elements (Fig. 1a and b). The elemental content was dominated by carbon with 58.85 atomic% and by oxygen with 40.89 atomic%. Negligible amounts of silicone (Si) and calcium (Ca) were also confirmed. This fibrous shape and the coarse porous nature of the sago hampas can act as a precursor for the formation of CNSs using neither any catalysts nor templates.

FT-IR study is used to ascertain the absorption bands associated with lignocelluloses such as cellulose, hemicelluloses and lignin in sago hampas (Fig. 1c). The characteristic hemicelluloses band observed around 1159 cm^{-1} may be ascribed to glycosidic linkage C–O–C and the cellulose absorption band can be observed at 1425 cm^{-1}.[31] A very week shoulder band observed around 1510 cm^{-1} can be assigned to the aromatic characteristic of lignin. This indicates the presence of low lignin content in sago hampas. The strong stretching vibration band observed around 1640 cm^{-1} can be assigned to carboxyl group (C=O) which is another evidence of a high content of oxygen present in the samples.[31] Along with this, the numerous absorption bands observed in the region 2900 and 1500–900 cm^{-1} are likely to originate from the structural diversity of celluloses and hemicelluloses[32] including C–OH and C–H functional groups. The bands at 1159 cm^{-1} and 1032 cm^{-1} suggests the presence of arabinosyl residues and α-glucan coming from the hemicelluloses.[33] Hence, the glycosidic linkages and hydroxyl groups of cellulose as well as the predominant ether bonds of hemicellulose and lignin as observed in this IR spectrum are in accordance with the previous literature suggesting a lignocellulosic compositions of about 64.4% cellulose, 25.1% hemicellulose and 10.5% lignin.[30] In the wide-angle XRD pattern of the sago hampas, two peaks were observed at 17.8° (d = 4.02 Å) and at 22.3° (d = 5.00 Å) corresponding to the 001 and 011 diffraction planes, respectively (Fig. 1d).[34] This is an indication of the microcrystalline nature of the cellulose.[35] Thus, the above characterization data highlight the high content of carbon and oxygen in sago hampas which will contribute to the formation of CNSs.

The raw sago hampas were pyrolyzed in tube furnace at two different temperatures (400 °C and 600 °C) for 2 hours under a continuous flow of N_2. The pyrolyzed products were then washed with a HCl solution and then rinsed with deionized water. When the applied temperature is 400 °C, the yield is around 20%. To investigate the morphology of the obtained CNSs, SEM and TEM observations were performed. As shown in the Fig. 2, most of the particles are spherical in shape, although some of them have irregular shapes. Similar results were reported in our previous study.[29a] The TEM analysis shows that the average CNSs particle size is 50 ± 5 nm and 65 ± 5 nm for a pyrolysis temperature of 600 °C and 400 °C, respectively. Thus, the particle size decreases when the applied pyrolysis temperature is increased. Similar observations were carried out through SEM imaging with an average particle size ranging from 60 to 70 nm when pyrolyzed at 600 °C and ranging from 80 to 90 nm when pyrolyzed at 400 °C. The particle size distribution histograms are presented in Fig. 2a-3 and b-3. The EDX analysis confirms that the relative carbon amounts for CNSs treated at 400 and 600 °C are 80.44 and 83.79 atomic%, respectively (Fig. S2 and S3†). Increasing the applied temperature improves the carbonization degree which results in the shrinkage of the particles. The details are discussed later.

The surface area was investigated by Brunauer–Emmett–Teller (BET) method. The BET surface area is 64 $m^2 g^{-1}$ 30 $m^2 g^{-1}$ for CNSs pyrolyzed at 600 °C and 400 °C, respectively. Hence,

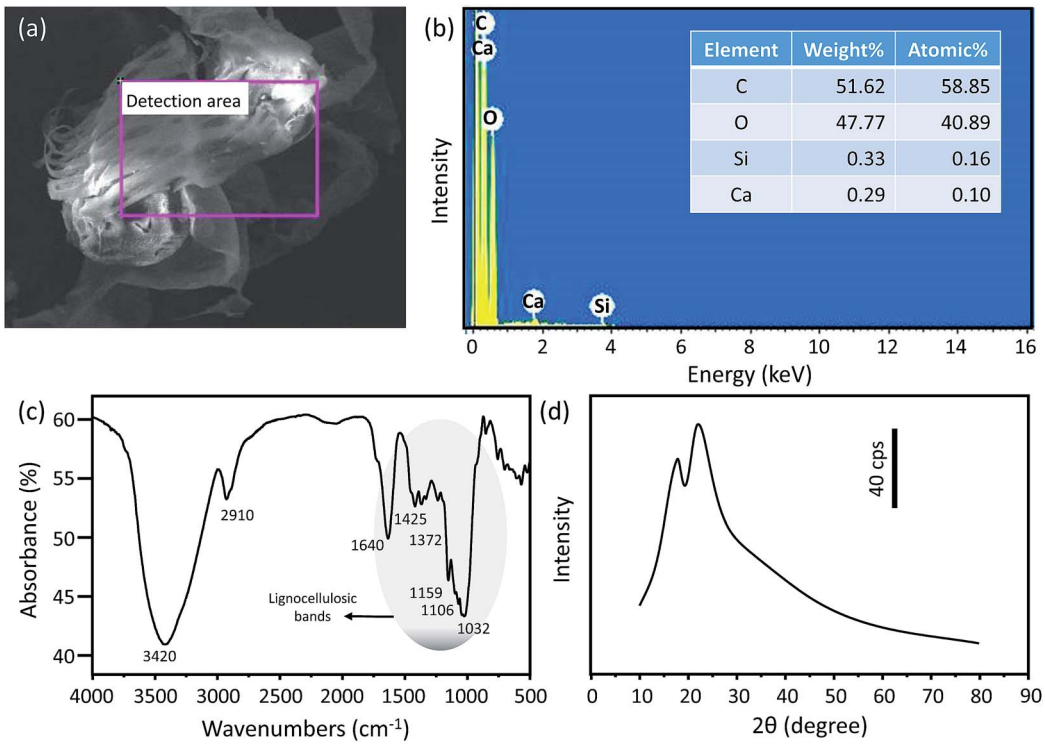

Fig. 1 (a) SEM image of raw sago hampas and (b) EDX spectrum taken from square area in (a). (c) FT-IR spectrum, and (d) wide-angle XRD pattern of raw sago hampas.

when the pyrolysis temperature is increased, the surface area is doubled. In our case, the CNSs are composed of dense carbon matrix without porous structures (as shown in Fig. 2a-1 and b-1). Therefore, the obtained surface area is mostly coming from the external particle surface roughness.

Wide-angle XRD patterns give important information regarding the graphitic structures of carbon as shown in Fig. 3a. The CNSs treated at 400 °C gave a main diffraction peak at 25.4° corresponding to the 002 plane which can be attributed to graphite (ICDD 10777164). The interlayer *d*-spacing (d_{002}),

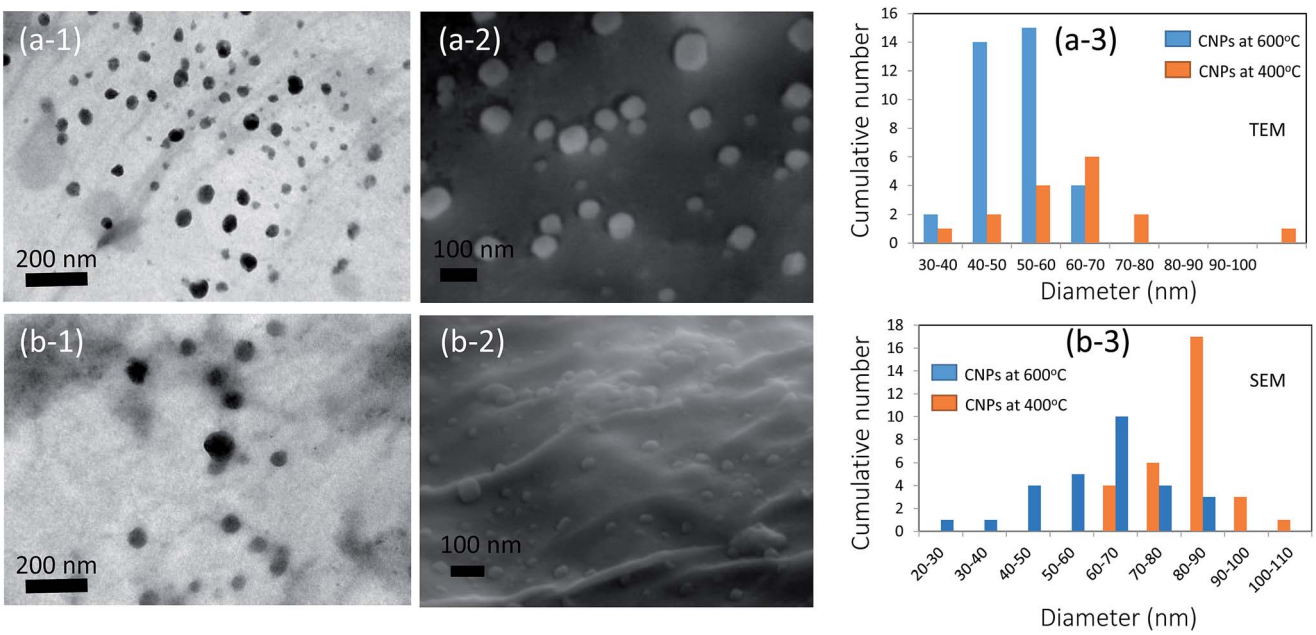

Fig. 2 (a-1 and b-1) TEM images, (a-2 and b-2) SEM images for CNSs treated at 600 °C and 400 °C; (a-3) the particle size distribution histograms for CNSs treated at 600 °C and 400 °C for TEM and (b-3) the particle size distribution histograms for CNSs treated at 600 °C and 400 °C for SEM.

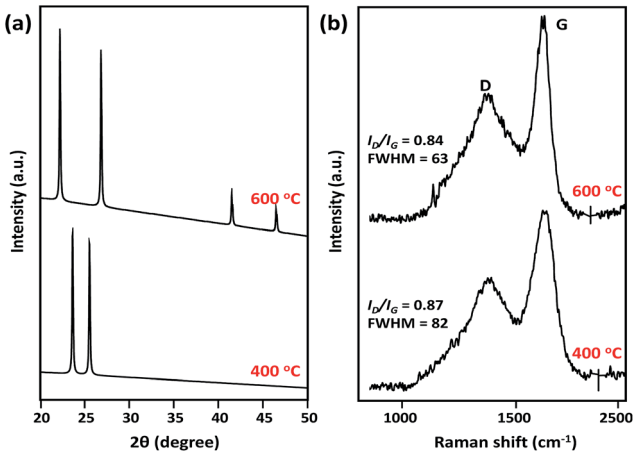

Fig. 3 (a) Wide-angle XRD patterns and (b) Raman spectra of CNSs treated at 600 °C and 400 °C.

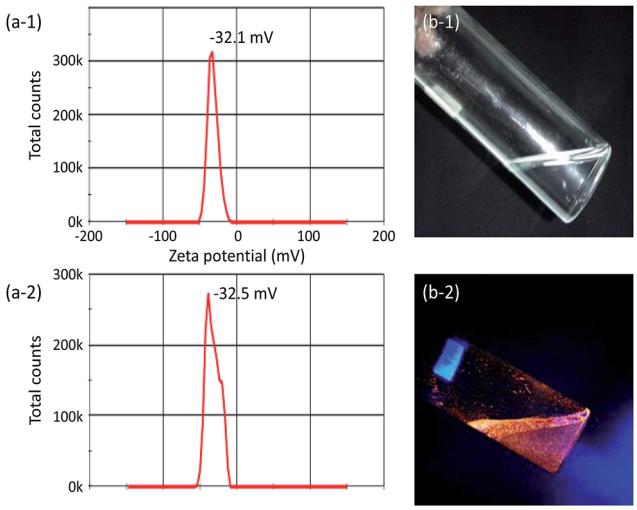

Fig. 4 (a) Zeta potential curves for aqueous solution of CNSs treated at (a-1) 600 °C and at (a-2) 400 °C. (b) Photographs of aqueous solution of CNSs treated at 400 °C (b-1) before and (b-2) after tagging.

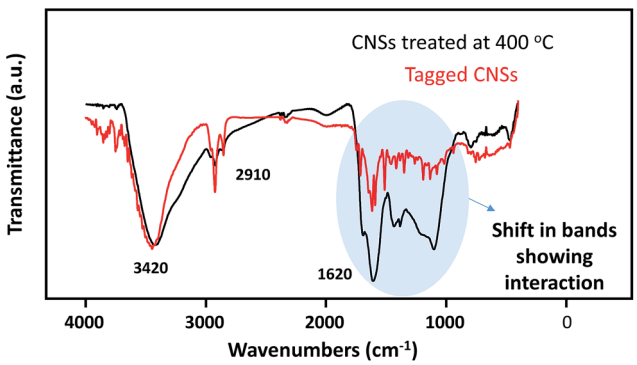

Fig. 5 FTIR spectra of CNSs treated at 400 °C before and after tagging.

which is used as a quantitative measurement of the graphitic character, is 3.50 Å.[36] In contrast, this peak is located at 26.8° (d_{002} = 3.32 Å) when the CNSs are treated at 600 °C (ICDD 10713739). At higher temperature, the interlayer *d*-spacing is slightly reduced. It is noted that additional peaks (at 23.5° for 400 °C and 22.2° for 600 °C) are also confirmed. These peaks are probably due to the highly crystalline cellulose fibres[35,37] which are formed from the hemicelluloses and celluloses of sago hampas. The most important point is that the XRD pattern for CNSs treated at 600 °C show two peaks at 41.5° and 46.4° which can be assigned to the 100 plane of graphite (*i.e.*, in-plane structure).[38] This peak was not observed in the case of CNSs treated at 400 °C. It is clear that high graphitic structure is realized after thermal treatment at 600 °C.

Raman spectroscopy is extremely useful in deducing the graphitic structure of carbon materials. Raman spectra of CNSs treated at 400 and 600 °C are presented in Fig. 3b. The carbon materials produce two main peaks denoted as the D- and G-bands. The D-band which is a diagnostic of disorder in the carbon structure is observed at 1397 and 1380 cm^{-1} for CNSs treated at 400 °C and 600 °C, respectively. The G-band, diagnostic of structural order, which is related to the sp^2 bonded carbon atoms from the stretching modes of C=C bonds, corresponding to the E_{2g} mode in graphite, is found at 1619 and 1624 cm^{-1} for CNSs treated at 400 °C and 600 °C, respectively.[39] Despite the different pyrolysis temperature, the peaks for D and G bands are similar. The graphitic character can further be assessed by the relative intensities of D- and G- bands (I_D/I_G).[40] In present case I_D/I_G ratio was found to be 0.87 and 0.84 at 400 °C and 600 °C, respectively. The full-width at half-maximum (FWHM) of the G-band is found to be 82 cm^{-1} and 63 cm^{-1} at 400 and 600 °C, respectively. The graphitic character increases as the FWHM value decreases with increasing the pyrolysis temperature. Thus, Raman results together with XRD results give an evidence of the strong graphitic character of the prepared CNSs treated at 600 °C.

In the FTIR spectra (Fig. S4†) of the obtained CNSs, the strong absorption band around 1620 cm^{-1} was assigned to the (C=O) bond of carbonyl group. The absorption bands around 3400, 2900 and 1500 cm^{-1} are assigned to the C–OH, C–H and C=C stretch of the carbon skeleton. We can observe large deviation in the shifts in the region 1500–900 cm^{-1} that are due to the lignocelluloses characteristics in sago hampas as precursor. As the pyrolysis temperature increases, the shifting of the peaks in the range of 1500–900 cm^{-1} is observed, due to the lignocellulosic material from the precursor degrading, thus increasing the graphitic degree.

Zeta potential values provide key information regarding the nanoparticles suspension stability and their cellular uptake.[41] In the present work, both type of CNSs showed a stable suspension behaviour as observed by their zeta potential values (Fig. 4a). CNSs pyrolyzed at 400 °C exhibited a zeta potential of −32.5 mV whereas CNSs obtained at 600 °C showed a potential of −32.1 mV in aqueous solution. The negative surface charge for both type of CNSs may be linked to the surface functional groups as observed in the FT-IR studies.

The CNSs have high zeta potential values, indicating a suitable stability for biological applications. Currently CNSs are

explored as interesting candidates for imaging applications for their size-guided cellular entry, low cytotoxicity profile and tunable emission properties.[42] Synthesized CNSs from biowaste with nano-scale particle size was expected to favour size related cellular entry. The CNSs pyrolised at 400 °C tagged with a fluorescent dye (coumarin 6) were examined[43] as they are in the size range favouring cellular uptake of nanoparticles.[44] The FTIR spectrum of the coumarin-6 tagged CNSs exhibited peak shifts. As shown in the Fig. 5, these peak shifts suggest that the fluorescent dye and the CNSs are interacting together. The suspension of the CNSs in aqueous solution is completely transparent (Fig. 4b-1) whereas the tagged CNSs have a red color (Fig. 4b-2), indicating their fluorescent nature after tagging. This gives a preliminary idea about the suitability of the present CNSs for cell imaging application.

Conclusions

In conclusion, this work describes a very simple single step fabrication of carbon nanospheres using biowaste materials. Obtained CNSs showed excellent particle size along with high zeta potential values. XRD and TEM data provide evidence of the CNSs quality and crystallographic properties. Fluorescent tagged CNS is promising candidate to become a low-cost probe for cell imaging applications. Detailed studies in this direction are in progress.

Acknowledgements

We sincerely acknowledge Ms Sumitha Gunasegaran and Ms Gan Siew Mei for kind help in synthesizing the nanospheres. This work was supported by Universiti Malaysia Sarawak Openg Research Chair and Center Of Excellent Grant [CoE-COESAR/PK07/07/2012(01)]. Ali Aldalbahi acknowledges the financial support by Deanship of Scientific Research, College of Science Research Center, King Saud University.

Notes and references

1 H. Yoon, S. Ko and J. Jang, *Chem. Commun.*, 2007, 1468–1470.
2 N. Yoshizawa, O. Tanaike, H. Hatori, K. Yoshikawa, A. Kondo and T. Abe, *Carbon*, 2006, **44**, 2558–2564.
3 R. Brayner, *Nano Today*, 2008, **3**, 48–55.
4 L. Cao, X. Wang, M. J. Meziani, F. Lu, H. Wang, P. G. Luo, Y. Lin, B. A. Harruff, L. M. Veca, D. Murray, S. Y. Xie and Y. P. Sun, *J. Am. Chem. Soc.*, 2007, **129**, 11318–11319.
5 Q. Quan, J. Xie, H. Gao, M. Yang, F. Zhang, G. Liu, X. Lin, A. Wang, H. S. Eden and S. Lee, *et al.*, *Mol. Pharm.*, 2011, **8**, 1669–1676.
6 I. Ali, *Curr. Cancer Drug Targets*, 2011, **11**, 130.
7 I. Ali, R. Uddin, K. Salim, M. A. Rather, W. A. Wani and A. Haque, *Curr. Cancer Drug Targets*, 2011, **11**, 135–146.
8 E. F. Kukovitsky, S. G. L'vov and N. A. Sainov, *Chem. Phys. Lett.*, 2000, **317**, 65–70.
9 A. K. Sinha, D. W. Hwang and L. P. Hwang, *Chem. Phys. Lett.*, 2000, **332**, 455–460.
10 R. L. Van der Wal, T. M. Ticich and V. E. Curtis, *J. Phys. Chem. B*, 2000, **104**, 11606–11611.
11 Y.-M. Shyu and F. Chau-Nan Hong, *Diamond Relat. Mater.*, 2001, **10**, 1241–1245.
12 P. M. Ajayan, J. M. Nugent, R. W. Siegel, B. Wei and P. Kohler-Redlich, *Nature*, 2000, **404**, 243.
13 Y. J. Jung, B. Wei, J. Nugent and P. M. Ajayan, *Carbon*, 2001, **39**, 2195–2201.
14 (*a*) D. Ugarte, *Nature*, 1992, **359**, 707; (*b*) Z. C. Kang and Z. L. Wang, *J. Mol. Catal. A: Chem.*, 1997, **118**, 215–222.
15 T. Stockli, J.-M. Bonard, A. Chatelain, Z. L. Wang and P. Stadelmann, *Phys. Rev. B: Condens. Matter Mater. Phys.*, 1998, **57**, 15599–15612.
16 R. Ryoo, S. H. Joo, M. Kruk and M. Jaroniec, *Adv. Mater.*, 2001, **13**, 677–681.
17 S. B. Yoon, K. Sohn, J. Y. Kim, C.-H. Shin, J.-S. Yu and T. Hyeon, *Adv. Mater.*, 2002, **14**, 19–21.
18 Y. Wu, P. Qiao, T. Chong and Z. Shen, *Adv. Mater.*, 2002, **14**, 64–67.
19 S. J. Yu, M. W. Kang, H. C. Chang, K. M. Chen and Y. C. Yu, *J. Am. Chem. Soc.*, 2005, **127**, 17604–17605.
20 A. B. Bourlinos, A. Stassinopoulos, D. Anglos, R. Zboril, V. Georgakilas and E. P. Giannelis, *Chem. Mater.*, 2008, **20**, 4539–4541.
21 F. Neugart, A. Zappe, F. Jelezko, C. Tietz, J. P. Boudou, A. Krueger and J. Wrachtrup, *Nano Lett.*, 2007, **7**(12), 3588–3591.
22 J. Lu, J. Yang, J. Wang, A. Lim, S. Wang and K. P. Loh, *ACS Nano*, 2009, **3**(8), 2367–2375.
23 T. Akiyama, N. Akae, M. Hayasaka and N. Ishikawa, *Metall. Mater. Trans. B*, 2004, **35**, 993–998.
24 S. L. Hu, K. Y. Niu, J. Sun, J. Yang, N. Q. Zhao and X. W. Du, *J Mater. Chem.*, 2009, **19**(4), 484–488.
25 H. Li, X. He, Y. Liu, H. Huang, S. Lian and S. T. Lee, *et. al.*, *Carbon*, 2011, **49**(2), 605–609.
26 K. Sudo and K. Shimizu, *J Appl. Polym. Sci.*, 1992, **44**(1), 127–134.
27 (*a*) J. Kadla, S. Kubo, R. Venditti, R. Gilbert, A. Compere and W. Griffith, *Carbon*, 2002, **40**(15), 2913–2920; (*b*) H. Aripin, L. Lestari, D. Ismail and S. Sabchevski, *Open Mater. Sci. J.*, 2010, **4**, 117–124.
28 (*a*) D. L. Dalluge, T. Daugaard, P. Johnston, N. Kuzhiyil, M. M. Wright and R. C. Brown, *Green Chem.*, 2014, **16**, 4144–4155; (*b*) Z. Jiang, T. He, J. Li and C. Hu, *Green Chem.*, 2014, **16**, 4257–4265.
29 (*a*) A. Kumar, G. Hegde, S. A. B. Abdul Manaf, Z. Ngaini and K. V. Sharma, *Chem. Commun.*, 2014, **50**(84), 12702–12705; (*b*) G. A. M. Ali, S. A. A. Manaf, A. Kumar, K. F. Chong and G. Hegde, *J. Phys. D: Appl. Phys.*, 2014, **47**, 495307, DOI: 10.1088/0022-3727/47/49/495307.
30 K. Kuroda, T. Ozawa and T. Ueno, *J. Agric. Food Chem.*, 2001, **49**, 1840–1847.
31 (*a*) S. F. Sim, M. Mohamed, N. A. Lu, M. I. Lu, N. S. P. Sarman and S. Samsudin, *Bioresources*, 2012, **7**(4), 5367–5380; (*b*) C. H. Cheng, J. Lehmann, J. E. Thies, S. D. Burton and M. H. Engelhard, *Org. Geochem.*, 2006, **37**, 1477–1488.

32 F. Peng, J. L. Ren, J. Bian and R. C. Sun, *J. Agric. Food Chem.*, 2009, **57**, 6305–6317.
33 M. Kacurakova, P. Capek, V. Sasinkova, N. Wellner and A. Ebringerova, *Carbohydr. Polym.*, 2000, **43**(2), 195–203.
34 Y. Nishiyama, J. Sugiyama, H. Chanzy and P. Langan, *J. Am. Chem. Soc.*, 2003, **125**, 14300–14306.
35 A. P. Mathew, K. Oksman and M. Sain, *J. Appl. Polym. Sci.*, 2005, **97**(5), 2014–2025.
36 Z. H. Li, D. C. Wu, Y. R. Linag, F. Xu and R. W. Fu, *Nanoscale*, 2013, **5**, 10824–10828.
37 (*a*) Z.-Y. Wu, C. Li, H.-W. Liang, J.-F. Chen and S.-H. Yu, *Angew. Chem., Int. Ed.*, 2013, **52**, 2925–2929; (*b*) D. Klemm, B. Heublein, H.-P. Fink and A. Bohn, *Angew. Chem., Int. Ed.*, 2005, **44**, 3358–3393.
38 S. Kuga, D.-Y. Kim, Y. Nishiyama and R. M. Brown, *Mol. Cryst. Liq. Cryst.*, 2002, **387**, 13–19.
39 (*a*) Y. Li, J. Chen, Q. Xu, L. He and Z. Chen, *J. Phys. Chem. C*, 2009, **113**, 10085–10089; (*b*) Y. Li, E. J. Lee, W. P. Cai, K. Y. Kim and S. O. Cho, *ACS Nano*, 2008, **2**, 1108–1112.
40 H.-S. Qian, F. M. Han, B. Zhang, Y.-C. Guo, J. Yue and B.-X. Peng, *Carbon*, 2004, **42**, 761–766.
41 (*a*) X. Zeng, W. Tao, L. Mei, L. Huang, C. Tan and S. S. Feng, *Biomaterials*, 2013, **34**, 6058–6067; (*b*) S. D. Perrault, C. Walkey, T. Jennings, H. C. Fischer and W. C. Chan, *Nano Lett.*, 2009, **9**, 1909–1915.
42 S. K. Bhunia, N. Pradhan and N. R. Jana, *ACS Appl. Mater. Interfaces*, 2014, **6**, 7672–7679.
43 Synthesis of fluorescent tagged CNPs: coumarin 6 dye was dissolved in dichloromethane and CNSs were suspended in the same solvent separately. The dye solution was added dropwise to the CNSs suspensions while continuous stirring. The solvent was evaporated by stirring overnight. The mixture was washed with dichloromethane to remove the unadsorbed dye present in the mixture. The remaining powdered mixture was washed with water and then dried at room temperature before being used for FTIR measurement. Fluorescent images were captured after UV exposure to the CNSs before and after tagging.
44 (*a*) F. Alexis, E. Pridgen, L. K. Molnar and O. C. Farokhzad, *Mol. Pharm.*, 2008, **5**, 505–515; (*b*) F. Yan, C. Zhang, Y. Zheng, L. Mei, L. Tang, C. Song, H. Sun and L. Huang, *Nanomedicine*, 2010, **6**, 170–178.